Proceedings of ASME Turbo Expo 2009: Power for Land, Sea and Air
GT2009
June 8-12, 2009, Orlando, Florida, USA

GT2009-60168

EVALUATING A THREE-DIMENSIONAL SLOT DESIGN FOR THE COMBUSTOR-TURBINE INTERFACE

D.G. Knost*
Mechanical Engineering
Virginia Tech
Blacksburg, Virginia 24061

K.A. Thole
Mechanical and Nuclear Engineering
The Pennsylvania State University
State College, Pennsylvania 16802

A. Duggleby
Mechanical Engineering
Texas A&M University
College Station, Texas 77843

ABSTRACT

As turbine inlet temperatures are pushed ever higher in an attempt to improve efficiency and power, it has become critical to cool component surfaces. One surface that is particularly difficult to treat because of the complex flow field that surrounds it is the nozzle guide vane endwall. Past studies have indicated that leakage bypass flow emerging from the combustor-turbine junction may be effectively harnessed for cooling purposes. When combined with endwall film-coolant injection, component service life may be significantly extended.

This paper presents results from a computational study investigating a three-dimensional slot geometry at the combustor-turbine interface. The downstream edge of the slot was scalloped using a simple periodic function intended to enhance thermal benefit to the endwall by manipulating coolant distribution. Effects of varying the slot geometry amplitude and phase were investigated along with the slot nominal width and upstream distance from the vane. Initial results indicate dramatic effects can be realized depending upon the scalloping used.

INTRODUCTION

Over the course of turbine technology development, inlet temperatures have increased well in excess of component thermal limits in the pursuit of improved performance and efficiency. Typically, relatively cool air is bled off of the compressor discharge, bypassing the combustor, and is used in internal cooling passages as well as injected through holes in component surfaces. Some bypass leakage flow escapes through gaps between components as a result of high pressure necessary to seal the wheelhouse and prevent hot core flow ingestion. Past studies demonstrate that leakage flow through the combustor-turbine endwall junction is useful for cooling, providing a buffer between the vane endwall surface and the hot combustor exit flow.

For traditional two-dimensional slots, the leakage flow emerges primarily between the airfoils and is typically swept toward the suction side of the passage leaving uncooled regions at the vane leading edge and along the pressure side. This paper introduces a three-dimensional slot geometry intended to influence leakage flow discharge and alter coolant coverage area and effectiveness. Effects of varying several geometric parameters are explored and results are related to a conventional, two-dimensional configuration. This paper precedes a statistical analysis and optimization of the parameters and highlights first order effects.

SUMMARY OF PAST LITERATURE

The endwall flowfield of a first stage turbine vane consists of unique features that contribute to high heat transfer and aerodynamic losses. Although there are slight differences in detail, flowfield studies by Langston et al. [1], Sharma and Butler [2], Goldstein and Spores [3], and others concur on the dominant structures in the endwall region for an approach flow that is uniform with a two-dimensional boundary layer. The incoming boundary layer on the endwall rolls up into a horseshoe vortex at the leading edge of the vane. The horseshoe vortex splits into suction and pressure side legs where the pressure side leg develops into a passage vortex as a result of the strong cross passage

*Address all correspondence to this author.

pressure gradient. These vortical structures and their interaction (generally termed "secondary flows") are sources of aerodynamic loss in the cascade; furthermore they sweep coolant from the endwall and increase endwall heat transfer coefficients.

Several studies have measured endwall heat transfer as a result of injection from a two-dimensional, flush slot upstream of the vane. Blair [4] measured adiabatic effectiveness levels and heat transfer coefficients for a range of blowing ratios through a flush slot placed just upstream of the leading edges of a single passage channel. One of the key findings was that the endwall adiabatic effectiveness distributions showed extreme variations across the vane gap. Much of the coolant was swept across the endwall toward the suction side corner resulting in reduced coolant near the pressure side. As the blowing ratio was increased, he found that the extent of the coolant coverage also increased. Measured heat transfer coefficients were similar between no slot and slot injection cases. In a later study by Granser and Schulenberg [5] similar adiabatic effectiveness results were reported with higher values occurring near the suction side of the vane.

A series of experiments report the results of various injection schemes upstream of a nozzle guide vane with a contoured endwall (Burd and Simon [6], Burd et al. [7], Oke, et al. [8, 9], and Oke and Simon [10]). In the studies presented by Burd and Simon [6], Burd et al. [7] and Oke, et al. [8] coolant was injected from an interrupted, flush slot that was inclined at 45° just upstream of their vane. Similar to others, they found that most of the slot coolant was directed toward the suction side at low slot flow conditions. As they increased the percentage of slot flow to 3.2% of the exit flow, measurements indicated increased coverage between the airfoils. In contrast, the study by Oke et al. [9] used a double row of film-cooling holes that were aligned with the flow direction and inclined at 45° with respect to the surface while maintaining nearly the same optimum 3% bleed flow of their previously described studies. They found that the jets lifted off the surface producing more mixing thereby resulting in a poorer thermal performance than the single slot. Oke and Simon [10] presented results from two upstream film-cooling rows with sections blocked to promote discharge in certain areas. They showed a vortex formed near the edge of the upstream film hole and moved toward the pressure side. The vortex was strengthened by increasing mass flow rate, impacting the pressure side of the vane farther upstream. An upstream hole configuration featuring a linear taper on the pressure and suction sides toward the center of the passage provided coolant to the leading edge at all blowing conditions while injection from a single row of holes with a linear taper on the suction side improved coolant supply to the pressure side at all blowing conditions. Pressure side coverage was higher than for the suction side at high mass flow ratios.

Roy et al. [11] compared their experimental measurements and computational predictions for a flush cooling slot that extended over only a portion of the pitch directly in front of the vane stagnation. Contrary to the previously discussed studies, their adiabatic effectiveness measurements showed that the coolant migrated toward the pressure side of the vane. Measurements indicated reduced values of local heat transfer coefficients at the leading edge when slot cooling was present relative to no slot cooling.

Lynch and Thole [12] presented measurements of adiabatic effectiveness and endwall shear stress as well as heat transfer coefficients for a flush slot with the vane geometry used in this work. The slot was moved upstream and contracted simulating axial thermal expansion. Results showed that coolant coverage area was similar for a fixed coolant mass flow rate at varying slot axial locations as the coverage area was dictated by secondary flows. However effectiveness levels within the passage were lowered for the slot further upstream as the coolant had longer to mix with the hot mainstream gases. Increasing coolant mass flow rate for a given slot width improved adiabatic effectiveness levels but also slightly increased heat transfer coefficients. More uniform coolant injection was also achieved with increased blowing as coolant momentum flux increased. This effect was amplified by reducing the slot width while maintaining a fixed coolant mass flow rate and resulted in broader coolant coverage within the passage. Overall, results indicated that for low slot momentum endwall secondary flows dictated coverage area while high momentum slot flow penetrated significantly downstream of the endwall separation line. Heat transfer coefficient augmentation was less severe for the contracted slot when compared with the nominal geometry. Net heat flux to the endwall was also reduced for the contracted slot compared to the nominal slot injecting at the same rate.

Colban et al. [13, 14] reported flow field and endwall effectiveness contours for a backward-facing slot with several different coolant exit conditions. Their measurements identified the presence of a tertiary vortex that developed in the vane passage due to a peaked total pressure profile in the near-wall region. For all of the conditions simulated, the effectiveness contours indicated the coolant from the slot was swept towards the suction surface.

Some studies have combined an upstream slot with film-cooling holes in the downstream endwall. Kost and Nicklas [15] and Nicklas [16] presented aerodynamic, heat transfer, and film-cooling effectiveness measurements from a transonic cascade. One of the most interesting results from this study was that they found for the slot flow alone, which was 1.3% of the passage mass flow, the horseshoe vortex became more intense. This increase in intensity resulted in the slot coolant being moved off of the endwall surface and heat transfer coefficients that were over three times that measured for no slot flow injection. They attributed the strengthening of the horseshoe vortex to the fact that for injection with no slot the boundary layer was already separated with fluid being turned away from the endwall at the injection location $0.2C_{ax}$. Given that the slot had a normal component

of velocity, injection at this location promoted the separation and enhanced the vortex. Their adiabatic effectiveness measurements showed higher values near the suction side of the vane due to the slot coolant migration. Kost and Mullaert [17] studied the same airfoil geometry, but moved the flush slot to $0.3C_{ax}$ upstream of the vane. They found for this configuration that slot flow stayed closer to the endwall and provided better cooling than flow from the slot located at $0.2C_{ax}$ upstream of the vane.

Knost and Thole [18, 19] presented computational and experimental results for combined slot flow and passage film-cooling. Increased blowing from the slot had a strong effect on the near-wall streamlines altering direction of injection from the film-cooling holes. This effect was particularly pronounced near the stagnation point and along the upstream portion of the pressure side. Higher flow turning was also exhibited within the passage.

Cardwell et al. [20] showed that coolant coverage area from the upstream slot leakage was dictated by coolant-to-mainstream momentum flux ratio with higher momentum flux leading to more uniform slot injection and coverage at the leading edge and along the pressure side. Local adiabatic effectiveness levels were demonstrated to be a strong function of coolant-to-mainstream mass flow ratio with adiabatic effectiveness levels improving at higher blowing rates.

While many have studied the effects of varying inlet conditions from fixed geometries, few have investigated varying the slot leakage geometry to manipulate coolant coverage and effectiveness. This work seeks to explore the possibilities for affecting leakage flow by varying parameters of a three-dimensional leakage geometry.

ENDWALL COOLING CONFIGURATION

The baseline endwall cooling configuration for this study, outlined in Table 1 and shown in Figure 1, is the same as presented by Knost and Thole [18]. It was developed with input from industrial partners. The scheme featured a flush upstream slot, simulating bypass leakage flow through the junction between the combustor and turbine endwalls, and 51 film-cooling holes. The original slot was two-dimensional and injected downstream in the axial direction at an inclination angle of 45 degrees with respect to the endwall. The slot centerline was stationed 0.42 axial chords upstream of the vane dynamic stagnation location to accommodate variations in the proposed new geometry without interfering with the film-cooling pattern.

Film-cooling holes were positioned along the vane endwall at the leading edge and in a pitchwise row upstream of the vane passage. Holes were arranged in axial rows within the passage along the vane pressure side and near the shoulder of the suction side. Holes at the leading edge and within the passage were spaced three hole diameters apart and injected downstream in the axial direction, while holes in the upstream row were spaced four hole diameters apart and directed toward the suction side injecting at 90 degrees with respect to the flow inlet direction. Two film-cooling holes near the pressure side trailing edge were directed at a compound angle of 45 degrees with respect to the axial direction. All film-cooling holes injected at a 30 degree inclination with respect to the endwall.

Table 1. Summary of Cooling Geometry Features

Feature	Scale 9x
Slot width [cm]	1.48
Slot length to width	1.8
Slot injection angle	45°
Upstream slot location	$-0.42C_{ax}$
Cooling hole diam [cm]	0.46
Cooling hole L/D	8.3
Hole injection angle	30°
p/d for leading edge holes	4/3
p/d for passage holes	3

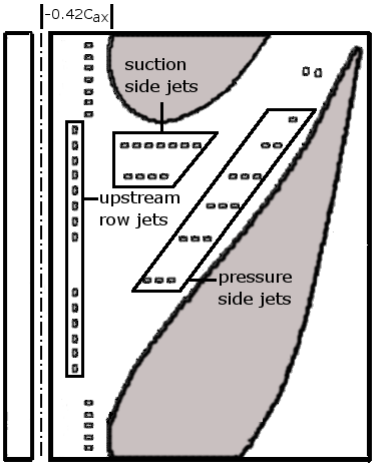

Figure 1. The baseline cooling configuration featured a two-dimensional slot and 51 film-cooling holes.

Three-Dimensional Slot Geometry

Traditionally the combustor-turbine slot geometry in published studies has been two-dimensional with the downstream edge of the combustor endwall and the upstream edge of the vane endwall flush and parallel. A three-dimensional combustor-turbine slot was investigated in this study utilizing a scalloped downstream edge intended to provide variable leakage flow me-

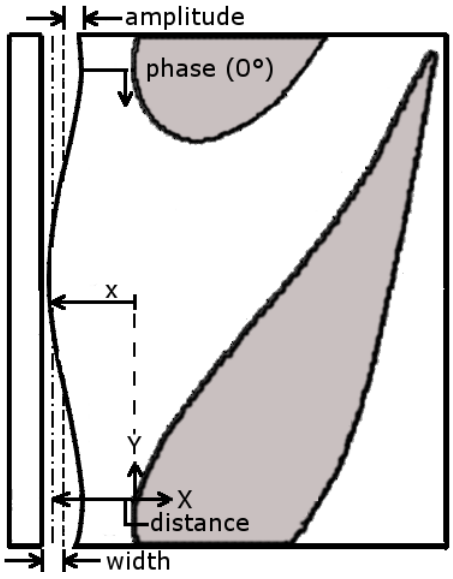

(a) plan view

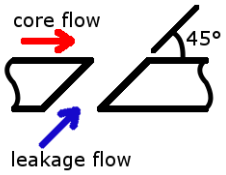

(b) slot side view

Figure 2. A three-dimensional slot with variable wave amplitude and phase, average width, and upstream distance was investigated.

tering across the vane pitch. As defined in Eq. 1 and illustrated in Figure 2(a), the downstream edge of the slot featured a cosine wave with four parameters: waveform amplitude, waveform phase, average slot width, and slot centerline upstream distance.

$$x = A\cos(2\pi y/\mathrm{P} + \phi) + \text{upstream dist} + \text{width}/2 \qquad (1)$$

A cosine was selected because of its smooth and continuous properties. As with the baseline geometry, the three-dimensional slot was flush and injected downstream at 45 degrees with respect to the endwall, illustrated in Figure 2(b). The film-cooling pattern remained unchanged from the baseline configuration and was included because film-holes are generally present within the passage and have been shown previously to have significant impact on endwall coolant distribution.

As mentioned in the literature review, previous studies have shown coolant from the slot to inject primarily near the center of the passage with little coolant emerging upstream of the vane stagnation. This leads to over-cooling in the center and

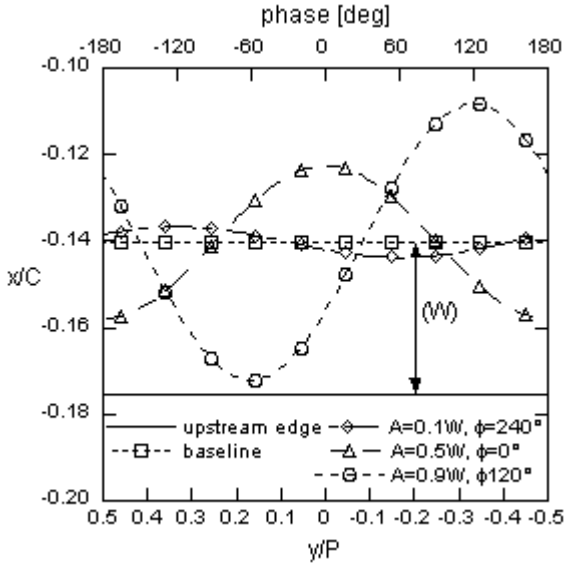

Figure 3. Total open area of the slot is independent of waveform phase and amplitude.

under-cooling at the leading edge and on the pressure side of the passage. The slot waveform amplitude was intended to restrict coolant mass flow in areas of low pressure through reduced flow area to moderate over-cooling. Additionally, it was thought that concentrating the slot open area near typical regions of low cooling would increase leakage flow over portions of the upstream endwall that are more difficult to cool. The waveform amplitude was also expected to have some effect on secondary flow development as less slot injection in low pressure areas may reduce the sink effect influence of the slot flow seen in previous studies [19] while more coolant injection should energize the boundary layer in areas where the flow stagnates. Amplitude was measured from the average upstream edge of the vane endwall, indicated by a dash-dash line in Figure 2(a), and expressed as a fraction of the average slot width.

The phase of the slot waveform was also investigated. Varying the waveform phase was expected to alter the leakage flow distribution shifting the slot coolant laterally across the endwall. Shifting phase was also expected to have some effect on secondary flow development as blowing non-uniformity was adjusted across the vane pitch. Phase was measured from a zero degree reference directly upstream of the vane stagnation.

Average slot width was varied as a global means of altering the coolant momentum flux ratio. The average slot width was computed as the distance between the upstream edge of the leakage geometry and the centerline of the downstream edge formed by the waveform, indicated by a dash-dash line in Figure 2(a). As shown in Figure 3, amplitude and phase have no net effect on total open area as the positive and negative areas about the wave-

form centerline cancel. Cardwell et al. [20] showed that varying slot width for a fixed coolant mass flow rate affected coolant coverage as higher momentum leakage flow penetrated beyond the endwall separation line of the horseshoe vortex yielding more uniform coolant coverage. A narrower average slot width with an open area concentration near the leading edge was expected to improve coolant coverage in difficult areas at the leading edge and along the pressure side for a fixed leakage rate and scale cooling levels for a fixed momentum flux ratio.

The final parameter under investigation was upstream distance to the nominal slot centerline. Upstream distance was measured from the axial location of the stagnation point to the centerline between the slot upstream edge and average downstream edge. The upstream distance location is shown as a dash-dot line in Figure 2(a). Previous studies indicated that coolant exits the slot in a non-uniform manner. This occurs because of the varying static pressure distribution over the endwall due to the presence of the downstream vanes. Lynch and Thole [12] showed that moving the slot further upstream improved slot coolant injection uniformity as the influence of the vane was reduced, but cooling levels within the passage were diminished as the coolant had longer to mix with the hot core flow. Varying upstream slot distance was intended to balance these effects to achieve coverage uniformity and adequate cooling levels.

COMPUTATIONAL DOMAIN AND METHODS

A plan view of the computational domain for this study is shown in Figure 4. The vane used was a commercial nozzle guide vane originally described by Radomsky and Thole [21]. It was two-dimensional with the midspan cross section modeled along the entire span. The vane and all other geometries in this study were scaled up by a factor of nine to allow comparison of results with any data acquired in the large-scale wind tunnel test section previously described by Knost and Thole [19]. The exit Reynolds number based on chord was matched to the engine.

Boundary Specification

The vane was divided at the dynamic stagnation location and trailing edge with a single passage modeled between. A velocity inlet boundary was specified one chord upstream of the passage. The domain was extended 0.1C beyond the trailing edge in the flow exit direction followed by an axial length of 0.25C to an outflow boundary. These locations were determined by Hermanson and Thole [22] to be free of pressure effects from the vane. Periodic boundary conditions were specified in the stagnation plane and beyond the trailing edge. The passage was modeled to midspan with an imposed symmetry condition to allow greater cell resolution within the domain. The slot and film-cooling holes were supplied from below by separate plenums with coolant mass flow rate and temperature imposed at mass

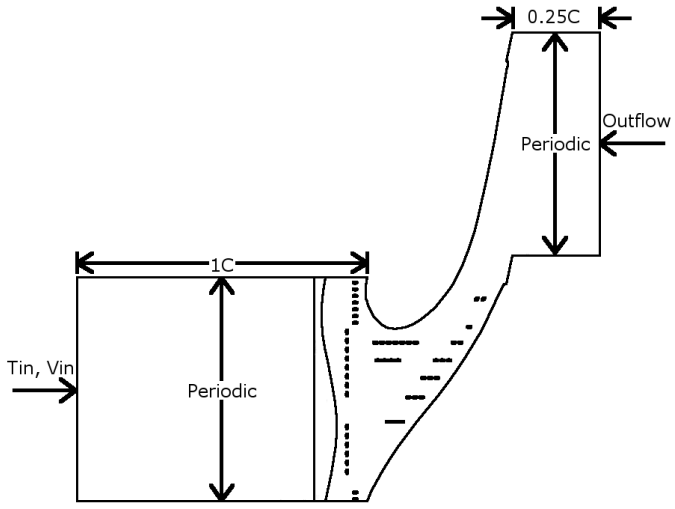

Figure 4. The computational domain featured a single passage modeled to midspan.

flow inlets. All walls were modeled as adiabatic with no slip except for the vertical plenum walls which were shear free. This was done to avoid viscous effects in the corners of the plenums.

Meshing and Grid Error Study

The solution domain was divided into multiple volumes to improve meshing ease. The mesh was a hybrid scheme incorporating structured hexahedral bricks, unstructured hexahedral bricks, pyramids, and tetrahedrons. Structured bricks were used from the velocity inlet to 0.3C upstream of the slot upstream edge and in the majority of the axial extension downstream of the trailing edge. This was done to conserve elements in areas where the flow was expected to be less complex. The passage was split at 30% span with unstructured bricks above this station and tetrahedrons below. The 30% span location was selected because it allowed an ample buffer above the the secondary flows which were expected to reside below 15% span based upon previous calculations and measurements. This stategy allowed much higher cell density in the lower portion of the passage with a more efficient hexahedral structure near midspan where the flow was expeceted to be largely two-dimensional. The slot and film-cooling holes were meshed individually with a minimum of approximately ten cells across any face where flow injected into the main passage. In addition the angle between outward facing normals of any two adjacent cells was limited to less than five degrees and the cell expansion rate was limited to ten percent between adjacent cells.

Five grids were initially evaluated to determine necessary mesh resolution in different parts of the passage. These grids were approximately 7 million, 8.7 million, 9.1 million, 15.8 million, and 22.8 million cells respectively. The 22.8 million cell grid served as a reference for error evaluation of the other four

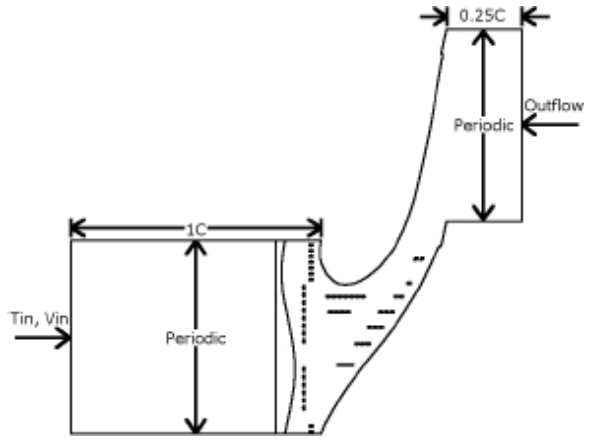

Figure 5. Each grid was sampled uniformly throughout the domain for error evaluation.

grids. The 8.7 million cell grid was adapted from the 7.0 million cell grid based upon computed values of y^+. The time required for this operation was prohibitive while the average error was still greater than for the similarly sized 9.1 million cell grid. This indicated that grid adaption was computationally inefficient compared to generating an initially finer grid.

Each grid was uniformly sampled in three dimensions at a spacing of approximately two film-cooling hole diameters as shown in Figure 5. The error at each location in temperature, pressure, velocity, and shear stress was computed with respect to the 22.8 million cell reference grid and the magnitude summed over the entire domain. The total error was then averaged and normalized to allow evaluation.

The thermal error, presented as average normalized temperature error, and the velocity component and magnitude errors are shown in Figure 6(a). It is seen that total grid error decreased as cell count (resolution) increased. Also, as stated previously, error was reduced more for the initially finer 9.1 million cell grid than for the similarly sized 8.7 million cell grid which was solution adapted from the coarsest grid. The average thermal error at a single sample location for the finest grid was less than 0.2% of the driving temperature difference ($\partial\eta, \partial\theta < 0.002$). The average velocity magnitude error was 2.5% of the inlet velocity while the z-component velocity errors were approximately an order of magnitude smaller than the x and y-component errors.

Average error magnitude was also computed in each spanwise sample plane to evaluate cell growth rate near the endwall as well as the division between tetrahedral and hexahedral cells at $z/S = 0.3$. The spanwise error summary for velocity magnitude is shown in Figure 6(b). Upon examination of the 7.0 million and 8.7 million cell grids it is clear that grid adaption occurred only below 10% span, where the complex secondary flows and coolant injection reside, and above 30% span where the cell type transition occured. Initial grid refinement to 9.1 million cells showed

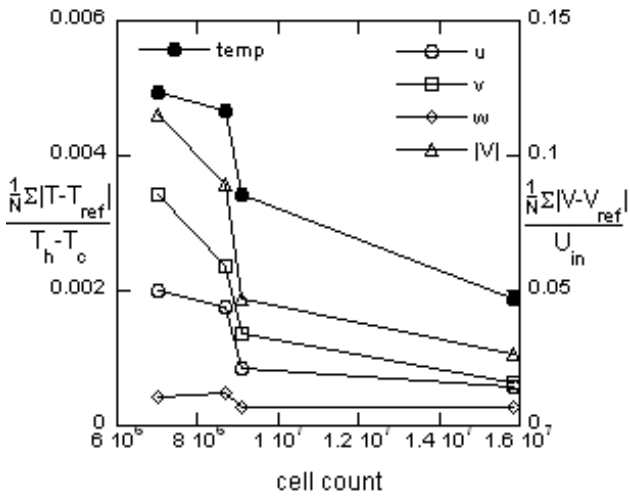

(a) total error

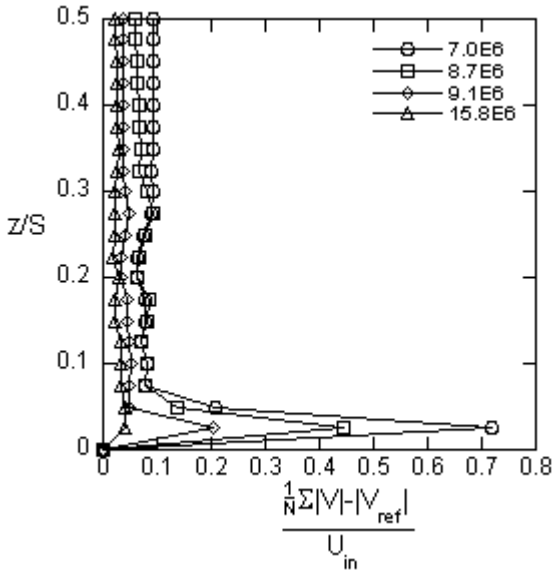

(b) spanwise error

Figure 6. Grid error was evaluated for convergence and uniformity with increasing cell count.

less error at all spanwise locations than the solution adapted grid but still an error spike at 2.5%span. This location typically coincides with the core of the secondary flows. Finally increasing the grid size to 15.8 million cells further reduced error at all spanwise locations and yielded a more uniform error distribution with an average velocity magnitude error of approximately 3% of the inlet velocity at all spanwise stations.

Error reduction was evaluated between meshes. The scheme

Table 2. Typical Cell Counts for Geometry Features

Feature	Cells
Inlet	38,000
Outlet	16,000
Film-cooling hole	45,000
Slot	300,000
Passage $z/S > 0.3$	33,000
Passage $z/S < 0.3$	8,000,000
Total	15,000,000

yielding the greatest relative gains and uniformity was selected for each sub-volume within the domain. Nominal cell counts for various features of the resulting production run grids are listed in Table 2. Production grids typically ranged from 14.5 to 16 million cells and fit comfortably on computing clusters with 32 GB of RAM.

Solution Procedure

The incompressible Reynolds-Averaged Navier-Stokes (RANS), energy, and turbulence equations were computed using the Fluent 6 pressure-based segregated solver. In this approach the momentum and pressure correction (continuity) equations are solved sequentially. The mass fluxes, pressure, and velocity fields are then updated from the pressure correction and additional scalar quantities such as energy and turbulence are computed. The segregated approach is memory efficient, since the segregated equations need only be stored one at a time, however solution convergence is relatively slow [23].

The RNG $k-\varepsilon$ turbulence model was utilized with enhanced wall functions. The RNG $k-\varepsilon$ turbulence model exhibits improved performance in comparison to the standard $k-\varepsilon$ model for complex shear flows and flows with high strain rates, swirl, and separation. Hermanson and Thole [22] showed good prediction of secondary flows with the RNG $k-\varepsilon$ turbulence model. The enhanced wall function option in Fluent employs a two-layer zonal model in the near-wall region where the laminar sublayer is resolved directly if grid resolution is fine enough ($y^+ \approx 1$) and a blending function is applied in the buffer layer [23].

The solution domain was initialized in three zones (front half of the passage, rear half of the passage, and plenums) and the laminar RANS equations were computed with first order discretization for 150 iterations to promote stability early in the solution procedure. The energy and turbulence equations were then included for an additional 150 iterations. Finally all equations were upgraded to second order discretization and computed for 1100 iterations. Solution residuals, area-averaged endwall temperature, mass-averaged total pressure at the inlet and outlet, lift, and drag coefficients were monitored at each iteration to evaluate solution convergence. Typical solution times ranged from 24-30 hours on ten 2.0GHz 64bit processors.

Table 3. Inlet Conditions for Various Cases

Inlet condition	Case #1	Case #2	Case #3
Inlet profile	Turb BL	Uniform	Peaked
Slot leakage rate	$0.5\%\dot{m}_{ex}$	$0.75\%\dot{m}_{ex}$	$1.0\%\dot{m}_{ex}$
Film-coolant rate	$0.5\%\dot{m}_{ex}$	$0.5\%\dot{m}_{ex}$	$0.5\%\dot{m}_{ex}$

INLET CONDITIONS

The baseline and three-dimensional slot geometries were evaluated for three different cases. The inlet conditions for the cases were distinguished by the inlet velocity and total pressure profiles as well as by the slot leakage flow rate. All inlet velocities had at turbulence intesity of 1.4% and turbulence integral length scale 0.067C. The film-coolant flow rate was fixed at 0.5% of the total exit mass flow rate to avoid confounding with variations in the leakage flow. The inlet temperature for all cases was uniform to insure changes in cooling levels were resulant only from variations in slot flow rate and distribution. The inlet conditions for these three cases are listed in Table 3. The cases were intended to encompass a wide range of inlet profiles and leakage flow rates.

The normalized inlet velocity and total pressure profiles for each case are shown in Figures 7(a) and 7(b). Hermanson and Thole [22] showed that secondary flow development was highly sensitive to the total pressure profile exiting the combustor. The turbulent inlet boundary layer they computed was selected for case #1 as the total pressure deficit in the boundary layer was identified as the primary factor in development of the horseshoe vortex. Additionally, the slot leakage rate was set at the lowest value under investigation, 0.5% of the total exit mass flow rate.

A uniform inlet velocity profile for case #2 corresponded to the inlet profile originally studied by Knost and Thole [18, 19]. When combined with a uniform inlet temperature this yielded a blunt total pressure profile at the domain inlet. Slot leakage was fixed at a moderate rate of 0.75% of the total exit mass flow rate.

Hermanson and Thole [22] argued that the turbulent boundary layer and uniform inlet temperature were not necessarily representative of combustor exit profiles during operation because of film-cooling and dilution blowing in the combustor. They proposed a total pressure profile which was peaked near the endwall as a result of much cooler fluid in the near-wall region. This led to a flow split part way up the span and a counter rotation of the flow above this station. Because it was undesirable in this study to introduce variations in coolant blowing anywhere but at the slot leakage geometry, a peaked near-wall velocity profile

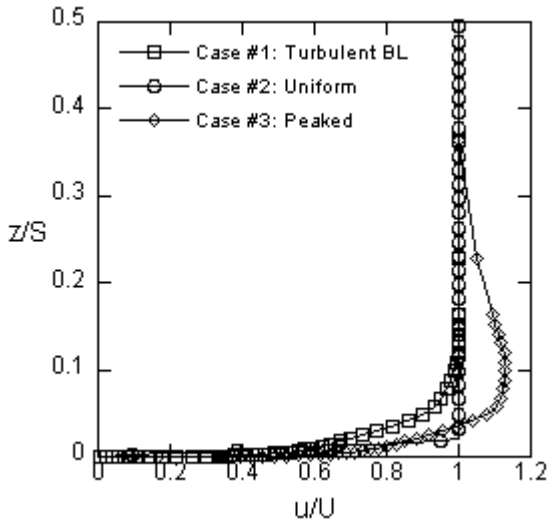

(a) velocity

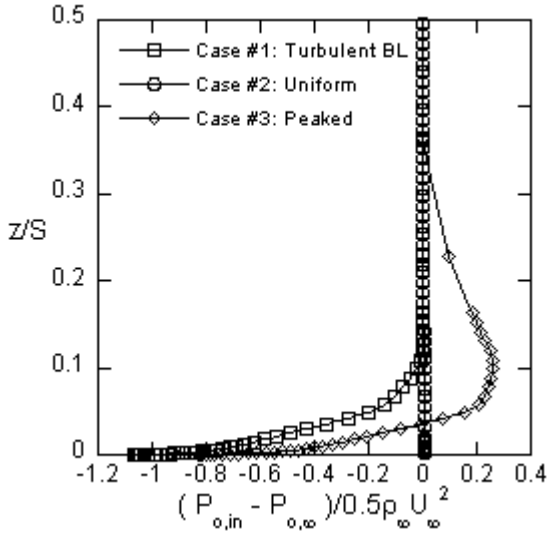

(b) total pressure

Figure 7. Normalized inlet profiles

was computed to match the peaked total pressure profile of Hermanson and Thole. This peaked profile was selected as the inlet condition for case #3 and combined with 1.0% $\dot{m}_{ex}$ slot leakage, the highest value investigated.

Mass-averaged coolant momentum flux ratio for the slot coolant was determined by the leakage flow rate for each case and the average slot width. Average momentum flux ratios were maintained while varying local values by manipulating scallop geometry. Mass-averaged momentum flux ratio could be matched between configurations while coolant flow rate varied by altering both average slot width and leakage rate. Varying

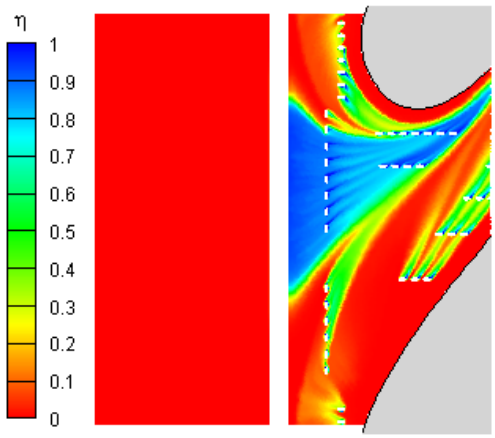

Figure 8. Baseline case with the slop at x/C_{ax} = -0.42.

only average width illuminated effects of altering momentum flux ratio for a fixed leakage rate.

DISCUSSION OF RESULTS

This paper supports a statistical study of the thermal and aerodynamic effects of the four slot parameters illustrated in Figure 2 [24, 25]. Selected cases are presented to illustrate primary effects of these parameters. Among these effects are:

- slot upstream distance affects leakage injection uniformity and cooling levels within the passage
- increasing waveform amplitude concentrates coolant injection location while shifting waveform phase shifts injection location
- contracting average slot width improves coolant coverage uniformity

Primary Effects of 3-D Slot Parameters

The baseline slot was a conventional, two-dimensional geometry injecting flow axially downstream at 45 degrees with respect to the endwall surface. Contours of adiabatic effectiveness for the baseline slot with the inlet conditions specified by case #1, consisting of 0.5% $\dot{m}_{ex}$ slot leakage flow and a turbulent boundary layer at the inlet, are shown in Figure 8. Adiabatic effectiveness is defined such that a value of unity indicates perfect cooling while a value of zero indicates no coolant present.

Coolant emerges from the slot in the center of the passage with no leakage flow present upstream of the vanes for the baseline geometry, as shown in Figure 8. On the suction side, the leading edge film-cooling jets are swept around the vane leaving an uncooled ring at the vane-endwall junction extending around the shoulder. Coolant from the pressure side leading edge holes exhibits low effectiveness and appears drawn upstream by the

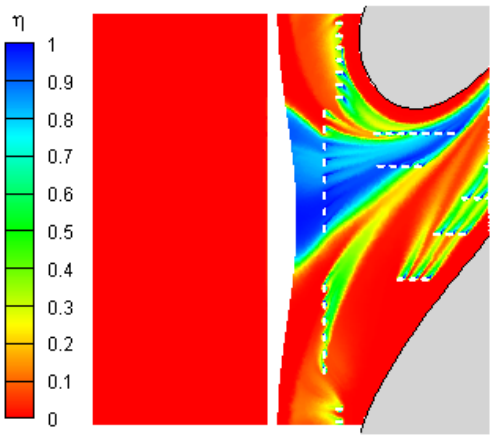

(a) x/C_{ax} = -0.42

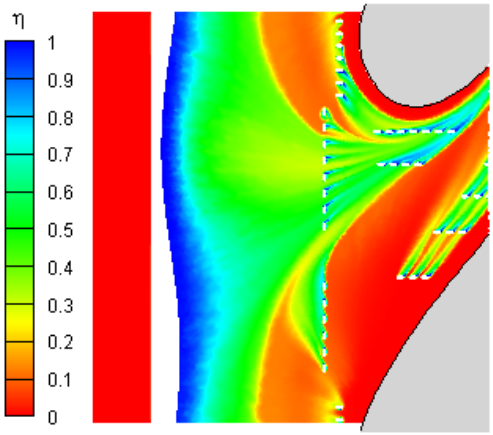

(b) x/C_{ax} = -1.0

Figure 9. Scalloped profiles with the slot at x/C_{ax} = -0.42 (a) and x/C_{ax} = -1.0 (b). Moving the slot upstream yields more uniform injection but reduces effectiveness levels within the passage. All configurations are shown at momentum flux ratio I=0.03 for the case #1 inlet conditions, and (a) is the baseline case.

leading edge horseshoe vortex. Additionally, the jet farthest upstream in the first row along the vane pressure side appears drawn toward the center of the passage.

Effects of scalloping the slot and moving its average centerline location axially upstream are illustrated in Figures 9(a) and 9(b). Both slot configurations have the same total flow area, leakage flow rate, and inlet profile as the baseline configuration of Figure 8. The average leakage momentum flux ratio for all three slot configurations is I=0.03. The average centerline location of the slot in Figure 9(a) is at $-0.42C_{ax}$, identical to the baseline configuration, while the average centerline location of the slot in Figure 9(b) is positioned one axial chord upstream of the vane stagnation.

For a waveform amplitude equal to half of the average slot width (A=0.5W), cooling levels and coverage area appear very similar to the baseline two-dimensional configuration for the same average momentum flux ratio and slot location. Coolant coverage appears narrower at the upstream film row yielding a slightly wider uncooled streak between the slot coverage region and the pressure side jets of the upstream row. Cooling levels remain marginally higher along the pressure side edge of the slot coverage area as local mass flow rate is slightly higher than from the two-dimensional geometry in this wider section of the slot. The film-cooling jets throughout the passage appear unaffected in comparison to Figure 8.

When the slot is moved upstream, coolant is seen to emerge across the entire width of the slot as the vane effect on endwall pressure distribution is reduced. Coolant injection exhibits a sinusoidal pattern indicating the coolant emerges primarily in the region of largest open area although the non-uniformity is not as pronounced as for the downstream location where coolant injects only in the center of the passage. Leakage flow from the upstream slot appears bounded by the legs of the horseshoe vortex and is funneled toward the center of the passage. The horseshoe vortex saddle point for this configuration is upstream of the slot location in Figure 9(a) indicating earlier formation. The pressure side leg of the horseshoe vortex draws the pressure side jets in the leading row upstream eliminating the uncooled streak between these jets and the slot coolant. Slot coverage immediately upstream of the leading film-cooling row and within the passage appears nearly identical to Figure 9(a), but cooling levels are significantly reduced as the coolant has far longer to mix with the hot core flow gases.

Contours of adiabatic effectiveness for a large amplitude slot geometry waveform are shown in Figures 10(a) and 10(b). The waveform amplitude is 90% of the average slot width while the phases are zero degrees (directly upstream of stagnation) and 120 degrees (shifted toward the suction side of the passage) respectively. The configuration in Figure 10(a) is shown for the inlet conditions specified by case #2 (Table 3, Figure 7). Both the average slot width and leakage flow rate in Figure 10(a) are increased by 50% over the values of Figure 8. The configuration in Figure 10(b) is shown for the inlet conditions specified by case #1 where the average slot width and leakage flow rate are identical to those of Figure 8. This yields nominally the same momemtum flux ratio, I=0.03. The slot is positioned one axial chord upstream of the vane stagnation in both configurations.

It is seen for both configurations that coolant injection is concentrated primarily in the region of largest open area while very little coolant emerges from the narrowest section of the slot. For zero phase, this induces a coolant coverage area with two peaks wrapping around the pressure and suction sides of the vane and an uncooled region upstream of the center of the passage. Some coolant is shown to penetrate beyond the endwall

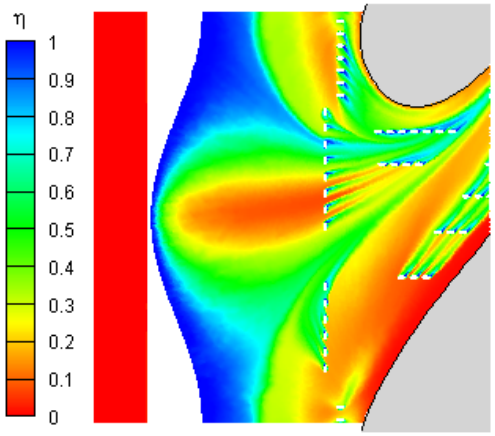

(a) 0° PHASE

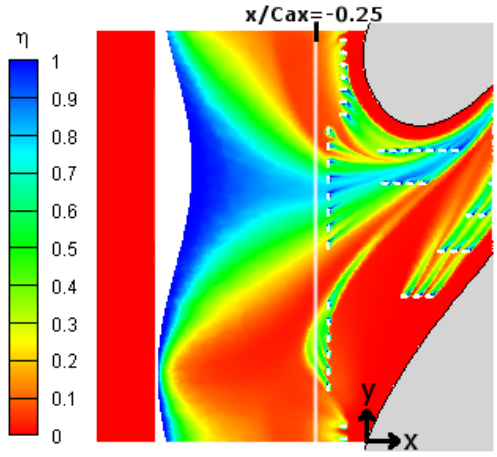

(b) 120° PHASE

Figure 10. Waveform amplitude concentrates coolant injection while phase shifts coverage area laterally (I=0.03, A=0.9W, x/C_{ax} = -1.0).

separation line, outlining cooling levels near unity, upstream of the leading edge. Leakage flow from the pressure side of the slot fills the space between the suction and pressure side jets of the upstream row broadening coverage area within the passage. Film-coolant from the suction side, leading edge holes advances very near to the vane leading edge-endwall junction while coolant from the pressure side holes of the upstream film-cooling row is drawn upstream and merges with the slot leakage flow.

When the phase is shifted in Figure 10(b) such that the open area is concentrated in the middle of the passage, very little coolant emerges toward the pressure side of the leading edge. Higher effectiveness levels are maintained within the passage in the slot coverage area near the vane shoulder in comparison to the zero phase configuration. The leading edge film-cooling jets are less effective leaving a thin uncooled ring at the leading edge-

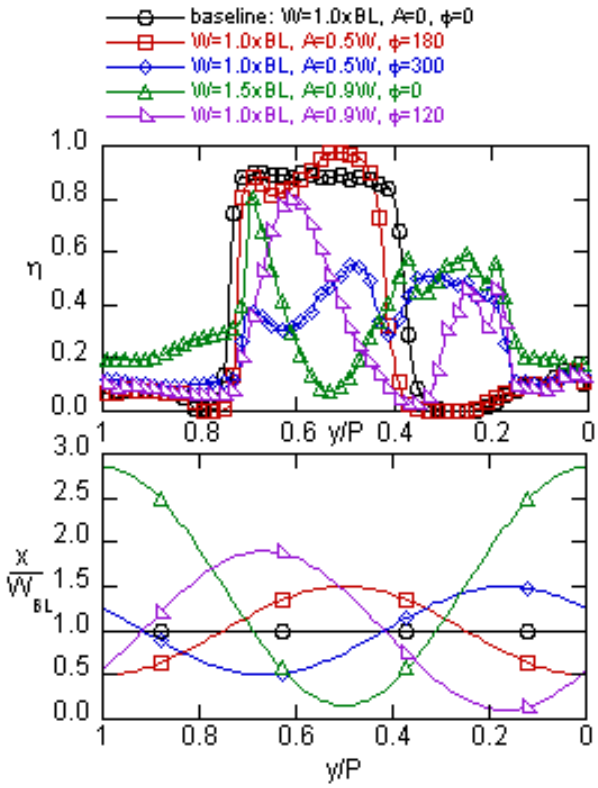

Figure 11. Pitchwise adiabatic effectiveness levels at x/C_{ax} = -0.25 (top) and slot geometry profiles (bottom) for I=0.03 cases.

endwall junction while the pressure side jets of the upstream row appear largely unaffected by the shifted slot coolant flow. As before, they are drawn upstream by the pressure side leg of the horseshoe vortex.

Pitchwise adiabatic effectiveness levels at x/C_{ax} = −0.25 for the five cases presented in Figures 8, 9 and 10 are shown in Figure 11. This station is slightly upstream of the leading film-cooling row as indicated by the white line in Figure 10(b). The configurations are listed in the legend in the order they were presented. The slot geometry profiles are shown in the lower portion of the figure for reference.

Cooling levels for the two configurations associated with Figures 8 and 9(a) appear very similar despite a slot geometry amplitude peak equal to half of the slot average width for the latter. The 180 degree waveform phase aligned the maximum slot open area in the center of the passage, a location where coolant naturally injects because of the low pressure. As noted previously the coolant coverage area is slightly narrower for the scalloped slot, but adiabatic effectiveness levels are a bit higher along the pressure side of the slot coverage range (y/P=0.5) where the slot open area is greatest. For both configurations the thermal

gradient is quite steep between the edge of the slot coverage and the adjacent portion of the endwall.

The width and shape of the lobe indicating slot coverage area associated with the configuration of Figure 9(b) appears similar to that for Figure 9(a). Both range from approximately $0.4 \leq y/P \leq 0.75$. The slot scallop amplitudes and widths were identical between these configurations, but the phase was shifted from 180 to 300 degrees. Cooling levels for the former configuration are significantly lower, though, as a result of the increased mixing length of the upstream slot location ($x/C_{ax} = -1.0$ vs. -0.42. There is a slight dip in cooling level near $y/P = 0.6$ associated with the narrow slot width at this station and then a rise because of coolant from the peaked region of the slot that is swept between the legs of the horseshoe vortex. On the pressure side of the endwall from $0.2 \leq y/P \leq 0.4$, cooling levels are significantly higher than for the first two configurations. This improvement results from the pressure side jets of the upstream row being drawn upstream as the horseshoe vortex forms further upstream. Cooling levels upstream of the leading edge are similarly low compared to the first two configurations.

Cooling levels upstream of the leading edge are nearly doubled for the configuration shown in Figure 10(a). This slot geometry was highly peaked with an amplitude equal to 90% of the average width and centered directly upstream of the leading edge. The average width was also 50% greater than for the other configurations. To match the coolant momentum flux ratio of the other configurations, the coolant flow rate was also increased by 50%. A spike in cooling level is seen at $y/P = 0.7$ from coolant at the leading edge that is swept around the suction side of the vane. Cooling levels fall rapidly towards the center of the passage, corresponding to the narrowest section of the slot, and then rise toward $y/P = 0.37$ because of leakage flow from the peak upstream of the adjacent leading edge. The primary slot coverage area between the two peaks indicate that the width between the legs of the horseshoe vortex does not vary significantly and that improved effectiveness levels at the leading edge result from leakage penetration beyond the horseshoe vortex. As with the other upstream slot locations, the pressure side jets of the leading row are drawn upstream improving cooling levels in the region between $0.2 \leq y/P \leq 0.4$.

Cooling levels for the configuration shown in Figure 10(b) indicate that leakage flow is contained between the legs of the horseshoe vortex from $0.4 \leq y/P \leq 0.75$, but the lobe is much narrower and the peak is shifted slightly toward the suction side of the passage because of the highly peaked slot geometry centered just to the suction side of the center of the passage. As with the configuration of Figure 10(a), maximum cooling levels approach those of the configurations where the slot was positioned much closer to the vane in contrast to the lower and more uniform cooling levels of the Figure 9(b) configuration.

Finally, cooling effectiveness contours illustrating the effect of expanding and contracting the average slot width for a fixed leakage rate are shown in Figures 12(a) and 12(b). Each configuration featured a slot waveform amplitude that was 50% of the average slot width, W, while the average slot width was expanded and contracted by 50% relative to the width of the baseline two-dimensional configuration. Both configurations are shown for the inlet conditions specified by case #3 with the high 1.0%$\dot{m}_{ex}$ flow rate and a peaked inlet total pressure profile. Contracting the slot increased the coolant momentum flux ratio by an order of magnitude.

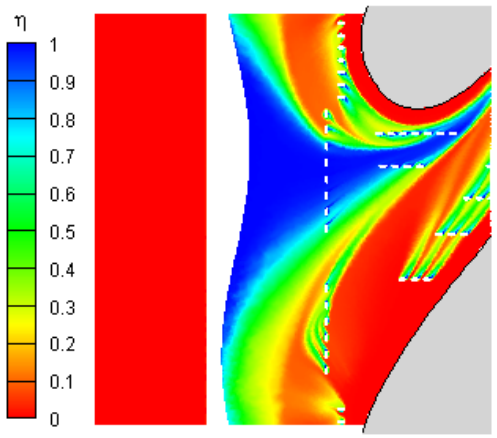

(a) WIDTH = 1.5xBaseline, I = 0.05

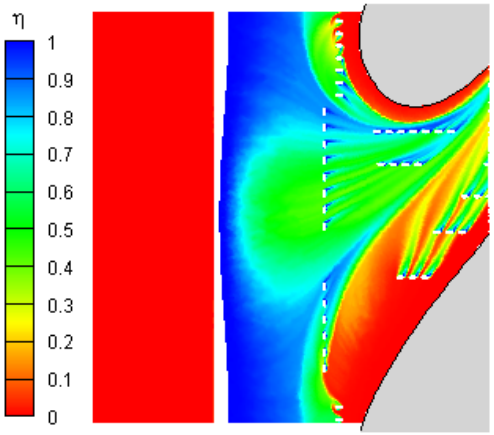

(b) WIDTH = 0.5xBaseline, I = 0.47

Figure 12. Contracting the slot improves coverage area at the leading edge and within the passage for a fixed leakage flow rate (A=0.5W, x/C_{ax} = -0.71, $\dot{m}_c$=1.0% $\dot{m}_{ex}$).

Slot coolant is seen to penetrate much closer to the vane leading edge for the contracted slot significantly reducing the uncooled area upstream of the vane. The saddle point of the horseshoe vortex also appears closer to the leading edge. Coverage area of the leading edge film-cooling jets appears unaltered.

Slot leakage coolant is bounded by the endwall separation lines and is funneled into the center of the passage for both configurations. The coverage area in the upstream portion of the passage is broader for the contracted configuration illustrated by a much narrower uncooled streak through the center of passage. The extended coolant coverage is attributed to the higher momentum flux of the injected leakage flow for the contracted slot. The upstream most jets along the pressure side film-cooling rows also appear drawn further across the passage for the contracted configuration indicating stronger endwall crossflow.

CONCLUSIONS

In modern gas turbines it is essential to provide cooling to component surfaces because of the extreme operating environment. One surface which is especially difficult to cool because of the complex flow field is the inlet nozzle guide vane endwall. Bypass leakage flow through the combustor-turbine endwall junction has been previously demonstrated to be useful in providing a protective coolant layer insulating portions of the endwall surface from the hot core flow.

A three-dimensional slot was investigated computationally to evaluate effects on endwall cooling. Grid error was assessed to quantify error magnitude and distribution and ensure that no large scale physics were unresolved. Effects of varying the slot waveform amplitude, phase, and upstream location were discussed for a fixed momentum flux ratio. Effects of varying the momentum ratio for a fixed coolant rate were also presented.

Primary effects of varying the slot parameters were as follows. Moving the slot centerline upstream facilitated more uniform coolant injection as the pressure variation across the endwall was reduced but also degraded cooling levels within the passage as the leakage flow had longer to mix with the hot core flow. Slot coolant coverage area was not significantly impacted. Increasing waveform amplitude was shown to concentrate coolant injection in regions with more open area while coolant flow from narrow portions of the slot was restricted. Adjusting waveform phase across the vane pitch shifted coolant injection location and altered coverage area both upstream and within the passage. Finally, expanding and contracting the average slot width altered coolant coverage area. The higher momentum leakage flow emerging from the narrower slot penetrated closer to the vane leading edge and exhibited broader coverage area in the upstream portion of the passage.

NOMENCLATURE

A waveform amplitude
C_{ax} vane axial chord
C_p pressure coefficient, $(p - p_{in}) / 0.5\rho U_{in}^2$
d hole diameter
D flow path diameter
k turbulent kinetic energy
I momentum flux ratio, $\rho_c V_c^2 / \rho_{in} V_{in}^2$
L flow path length
$\dot{m}$ mass flow rate
p pressure, hole pitch
P vane pitch
P_o total pressure
S vane span
T temperature
u,v,w streamwise, stream normal, wall normal local flow velocities
U inlet flow velocity
V velocity
W flow path width
y^+ non-dimensional relative distance
x,y,z local coordinate system
X,Y,Z global coordinate system

Greek

ε turbulent kinetic energy dissipation rate
η endwall adiabatic effectiveness, $(T_{in} - T) / (T_{in} - T_c)$
ϕ waveform phase
ρ density

Subscripts

BL baseline
c coolant
comp component
ex domain exit
in domain inlet
ref reference

REFERENCES

[1] Langston, L. S., 1980. "Crossflows In a Turbine Cascade Passage". *Journal of Engineering for Power,* **102**, pp. 866–874.

[2] Sharma, O. P., and Butler, T. L., 1987. "Predictions of Endwall Losses and Secondary Flows in Axial Turbine Cascades". *J. of Turbomachinery,* **109**, pp. 229–236.

[3] Goldstein, R. J., and Spores, R. A., 1988. "Turbulent Transport on the Endwall in the Region Between Adjacent Turbine Blades". *J. of Heat Transfer,* **110**, pp. 862–869.

[4] Blair, M. F., 1974. "An Experimental Study of Heat Transfer and Film Cooling on Large-Scale Turbine Endwalls". *J. of Heat Transfer*, pp. 524–529.

[5] Granser, D., and Schulenberg, T., 1990. "Prediction and Measurement of Film Cooling Effectiveness for a First-Stage Turbine Vane Shroud". 90-GT-95.

[6] Burd, S. W., and Simon, T. W., 2000. "Effects of Slot Bleed Injection Over a Contoured Endwall on Nozzle Guide Vane Cooling Performance: Part I: Flow Field Measurements". 2000-GT-199.

[7] Burd, S. W., Satterness, C. J., and Simon, T. W., 2000. "Effects of Slot Bleed Injection Over a Contoured Endwall on Nozzle Guide Vane Cooling Performance: Part II: Thermal Measurements". 2000-GT-200.

[8] Oke, R., Simon, T. W., Burd, S. W., and Vahlberg, R., 2000. "Measurements in a Turbine Cascade Over a Contoured Endwall: Discrete Hole Injection of Bleed Flow". 2000-GT-214.

[9] Oke, R., Simon, T., Shih, T., Zhu, B., Lin, Y. L., and Chyu, M., 2001. "Measurements Over a Film-Cooled, Contoured Endwall with Various Coolant Injection Rates". 2001-GT-140.

[10] Oke, R., and Simon, T., 2002. "Film-Cooling Experiments with Flow Introduced Upstream of a First Stage Nozzle Guide Vane Through Slots of Various Geometries". GT2002-30169.

[11] Roy, R. P., Squires, K. D., Gerendas, M., Song, S., Howe, W. J., and Ansari, A., 2000. "Flow and Heat Transfer at the Hub Endwall of Inlet Vane Passages - Experiments and Simulations". 2000-GT-198.

[12] Lynch, S. P., and Thole, K. A., 2007. "The Effect of Combustor-Turbine Interface Gap Leakage on the Endwall Heat Transfer for a Nozzle Guide Vane". GT2007-27867.

[13] Colban, W. F., Thole, K. A., and Zess, G., 2002. "Combustor-Turbine Interface Studies: Part 1: Endwall Measurements". *J. of Turbomachinery,* **125**, pp. 193–202.

[14] Colban, W. F., Lethander, A. T., Thole, K. A., and Zess, G., 2002. "Combustor-Turbine Interface Studies: Part 1: Flow and Thermal Field Measurements". *J. of Turbomachinery,* **125**, pp. 203–209.

[15] Kost, F., and Nicklas, M., 2001. "Film-Cooled Turbine Endwall in a Transonic Flow Field: Part I - Aerodynamic Measurements". 2001-GT-0145.

[16] Nicklas, M., 2001. "Film-Cooled Turbine Endwall in a Transonic Flow Field: Part II - Heat Transfer and Film-Cooling Effectiveness Measurements". 2001-GT-0146.

[17] Kost, F., and Mullaert, A., 2006. "Migration of Film-Coolant from Slot and Hole Ejection at a Turbine Vane Endwall". GT2006-90355.

[18] Knost, D. G., and Thole, K. A., 2005. "Computational predictions of endwall film-cooling for a first stage vane". *International J. of Turbo and Jet Engines,* **22**, pp. 41–58.

[19] Knost, D. G., and Thole, K. A., 2005. "Adiabatic Effectiveness Measurements of Endwall Film-Cooling for a First Stage Vane". *J. of Turbomachinery,* **127**, pp. 297–305.

[20] Cardwell, N., Sundaram, N., and Thole, K. A., 2006. "The Effects of Varying the Combustor-Turbine Gap". GT2006-90089.

[21] Radomsky, R. W., and Thole, K. A., 2000. "Flowfield Measurements for a Highly Turbulent Flow in a Stator Vane Passage". *J. of Turbomachinery,* **122**, pp. 255–262.

[22] Hermanson, K., and Thole, K. A., 2000. "Effect of Inlet Profiles on Endwall Secondary Flows". *J. of Propulsion and Power,* **16**, pp. 286–296.

[23] Fluent Inc., 2006. *Fluent 6.3 User's Guide*. (Fluent Inc: New Hampshire).

[24] Knost, D. G., Thole, K. A., and Duggleby, A., 2010. Parametric Investigation of the Combustor-Turbine Interface Leakage Geometry: Part I - Thermal Optimization.

[25] Knost, D. G., Thole, K. A., and Duggleby, A., 2010. Parametric Investigation of the Combustor-Turbine Interface Leakage Geometry: Part II - Secondary Flows.